Modeling ultrashort-pulse laser ablation of dielectric materials

B. H. Christensen* and P. Balling†
Department of Physics and Astronomy, University of Aarhus, DK-8000 Aarhus C, Denmark
(Received 10 October 2008; revised manuscript received 17 February 2009; published 15 April 2009)

An approach to modeling ablation thresholds and depths in dielectric materials is proposed. The model is based on the multiple-rate-equation description suggested by Rethfeld [Phys. Rev. Lett. **92**, 187401 (2004)]. This model has been extended to include a description of the propagation of the light into the dielectric sample. The generic model is based on only a few experimental quantities that characterize the native material. A Drude model describing the evolution of the dielectric constant owing to an excitation of the electrons in the material is applied. The model is compared to experimental ablation data for different dielectric materials from the literature.

DOI: 10.1103/PhysRevB.79.155424 PACS number(s): 79.20.Ds, 52.38.Mf, 78.47.−p, 61.80.Ba

I. INTRODUCTION TO ABLATION OF DIELECTRIC MATERIALS

The interaction of ultrashort laser pulses with dielectric materials is a subject of significant interest, both from a fundamental perspective as an area for the investigation of strong, short electromagnetic pulses with matter, and for more practical reasons related to laser-induced material modifications as, e.g., the writing of index changes or micromachining.

The underlying physics in the ablation process of metals and dielectric materials is quite dissimilar. Metals are characterized by a large density of quasi-free-electrons that may absorb the incoming radiation, and much of the dynamics following excitation by ultrashort laser pulses is captured by advanced thermal models as, e.g., the two-temperature model.[2,3] Dielectric materials are often transparent to the light, and typically conduction-band electrons must first be generated by the light to be able to start the ablation process. In the following the conduction-band electrons will be referred to as free electrons.

The initial generation of free electrons in a dielectric material can be considered to occur via strong-field ionization as described for instance in the Keldysh picture.[4] When the generation of free electrons is initiated, collision processes can occur, and multiplication can take place by impact ionization, while the electrons can be heated due to inverse Bremsstrahlung. With free electrons present, absorption of the remaining part of the light pulse can start to take place, which is leading to a further heating of the excited electrons and thereby the dielectric medium starts to behave as a metal.

The abrupt change from an insulator to a material, where a large fraction of the electrons are excited to the conduction band, introduces significant changes in the refractive index. Especially the imaginary part of the refractive index is changed as this was vanishing before the laser illumination of the sample. These changes will be discussed and modeled so that the propagation of the light in the laser-excited medium can be accounted for. By employing an appropriate ablation criterion based on the material excitation at the end of a laser pulse, the ablation depth as a function of the incoming laser fluence can be obtained.

II. MULTIPLE RATE EQUATION

There has been a lot of effort in modeling the ablation threshold of dielectrics. The level of detail has varied considerably where the most advanced models are computationally demanding. The most straightforward approach was proposed by Stuart *et al.*[5] where the model is a single rate equation (SRE) describing the density of excited electrons, n, which is given as

$$\frac{\partial n}{\partial t} = \dot{n}_{pi} + \beta(I)n. \tag{1}$$

Here $\dot{n}_{pi}$ is the strong-field ionization term and $\beta(I)$ is an intensity-dependent impact ionization rate. A more elaborate model, including the physical processes involved in the excitation process in greater detail, was proposed by Kaiser *et al.*,[6] but at the cost of solving 325 nonlinear, coupled differential equations. In a recent paper, the results of an impressive first-principles electron-dynamics simulation of optical breakdown using time-dependent density-functional theory was presented.[7]

Such advanced models are at present not suitable for an extension to include propagation effects into the bulk due to the complexity and thereby the high demand on computational power. As a consequence Rethfeld[1] proposed a multiple-rate-equation (MRE) model, which was including the most dominant physical effects in the model proposed by Kaiser *et al.*,[6] but without the high demand on the computation time.

In the MRE model, electrons in the valence band are excited to the conduction band by strong-field ionization.[4,6] This process is then followed by one-photon excitation leading to an increased energy of the conduction-band electrons. When the energy of an electron in the conduction band is sufficiently high, impact ionization can occur with a rate α, and two electrons with a low kinetic energy are generated. In the MRE model this has been described by introducing discrete levels in the conduction band spaced with the photon energy of the incident light. The following equations for the density of free electrons in these levels are then proposed to describe the excitation process:[1,8]

$$\frac{\partial n_1}{\partial t} = \dot{n}_{pi} - W_{1pt} n_1 + 2\alpha n_i,$$

$$\frac{\partial n_2}{\partial t} = W_{1pt} n_1 - W_{1pt} n_2,$$

$$\frac{\partial n_{i-1}}{\partial t} = W_{1pt} n_{i-2} - W_{1pt} n_{i-1},$$

$$\frac{\partial n_i}{\partial t} = W_{1pt} n_{i-1} - \alpha n_i. \tag{2}$$

Note that these equations can be added up to provide a form, which looks much like the single-rate equation,

$$\frac{dn_{\text{total}}}{dt} = \dot{n}_{pi}(E_L) + \alpha n_i. \tag{3}$$

In Eq. (3) the first term describes strong-field ionization and the last term takes impact ionization into account. These two factors are considered the most dominant in excitation of electrons in dielectrics. In the rate equations the one-photon excitation rate W_{1pt} is included to simulate the populations in the intermediate levels.

In a comparison between the models based on SRE and MRE, it should be noted that strong-field ionization generates electrons with a low kinetic energy, whereas impact ionization is only performed by electrons with a sufficiently high kinetic energy. The major advantage of the MRE model is that only electrons with sufficiently high kinetic energies to fulfill both energy and momentum conservation in the ionization process contribute to impact ionization in the last term of Eq. (3). This is in contrast to the SRE in Eq. (1), where all electrons are assumed to contribute to impact ionization.

III. NUMERICAL MODELING

In this section, it will be described how the simulations of the MRE model are expanded to include propagation of the optical fields in a one-dimensional model, meaning that a parallel beam with a uniform transverse intensity distribution has been assumed. In the simulation the excited electrons are assumed to behave as a free-electron gas described by the Drude model. All propagation effects will then be described from the complex refractive index $\tilde{k}=k+i\kappa$ here denoted by $\tilde{k}$ to avoid confusion with the electron densities denoted by n. The major propagation effects in the model are reflection from the front surface and absorption of light by the excited electrons. Note that this requires the merging of a microscopic model, describing the electron excitation, and a macroscopic model for the dielectric properties of the excited material. A generic model based on only a few material parameters is attractive, and this simulation is applying only (i) the band gap of the dielectric material and (ii) the initial refractive index as relevant material parameters, while the total electron density is kept constant at $n_{\text{tot}}=10^{29}$ m^{-3}.

A. Setting up the model

More specifically, following the scheme from Eq. (2), rate equations for the electron densities are set up, in which the excited electrons are modeled by a number of discrete levels separated by the photon energy. The electron densities in the individual levels are described by rate equations where the spatially and temporally dependent electron density in the jth excited level is written as n_j. Note that the strong electromagnetic field shifts all the excited (conduction band) levels by an amount equal to the ponderomotive energy, which is expressed by $U_p=e^2E_l^2/(4m_{\text{redu}}\omega_l^2)$. Here e, E_l, ω_l, and m_{redu} are the charge of the electron, the electric field amplitude, the laser frequency, and the reduced effective mass of the electron in the conduction band and the hole in the valence band, which in the main part of this paper will be approximated with half the electron mass $m_e/2$.[1]

The incident light is assumed to be a temporally Gaussian pulse. When the light is incident on the sample it will start to experience losses owing initially to multiphoton processes followed by single-photon absorption in the free-electron plasma. These effects are included in the description of the light as losses. The light is in the simulation described in a photon picture with the photon density given by $u(t,z)$ which is also dependent on both time and space. The modeling of the light and the losses will be discussed in detail in Sec. III D.

The coupled differential equations for the levels of excited electrons can be solved as a function of time and the depth into the material. The MRE model proposed by Rethfeld is modified in several ways. The one-photon absorption is replaced by Drude plasma absorption and in addition changes have been made to the distribution of the electrons originating from impact ionization to conserve energy and finally a saturation term has been included. The differential equations for the electron levels can then be written in the following way:

$$\frac{\partial n_1}{\partial t} = \dot{n}_{pi}(u)\frac{n_{\text{val}}}{n_{\text{tot}}} - W_{pl} n_1 + \alpha\frac{n_{\text{val}}}{n_{\text{tot}}}\sum_{j=1}^{j_{\text{crit}}} n_j \Theta\left(j\hbar\omega_L - \frac{3}{2}E_{\text{corr}}\right)\Upsilon(\Delta E), \tag{4}$$

$$\frac{\partial n_2}{\partial t} = W_{pl}(n_1 - n_2) + \alpha\frac{n_{\text{val}}}{n_{\text{tot}}}\sum_{j=1}^{j_{\text{crit}}} n_j \Theta\left(j\hbar\omega_L - \frac{3}{2}E_{\text{corr}}\right) \times \Upsilon(\Delta E - 1), \tag{5}$$

$$\frac{\partial n_{j_{\text{crit}}-1}}{\partial t} = W_{pl}(n_{j_{\text{crit}}-2} - n_{j_{\text{crit}}-1}) + \alpha\frac{n_{\text{val}}}{n_{\text{tot}}}\sum_{j=1}^{j_{\text{crit}}} n_j \Theta\left(j\hbar\omega_L - \frac{3}{2}E_{\text{corr}}\right) \times \Upsilon[\Delta E - (j_{\text{crit}} - 2)], \tag{6}$$

$$\frac{\partial n_{j_{\text{crit}}}}{\partial t} = W_{pl} n_{j_{\text{crit}}-1} - \alpha\frac{n_{\text{val}}}{n_{\text{tot}}}\Theta\left(j_{\text{crit}}\hbar\omega_L - \frac{3}{2}E_{\text{corr}}\right). \tag{7}$$

The function Υ, which is relevant in connection with the impact ionization, is defined as

$$\Upsilon(x) = \begin{cases} 2 & \text{for } -0.25 \le x \le 0.25 \\ 1 & \text{for } 0.25 < x < 0.75 \\ 0 & \text{else.} \end{cases} \quad (8)$$

It should be emphasized that in the rate equations as written above, the level j_{crit} is assumed to be above the threshold for impact ionization whereas the other levels are below. Due to the ponderomotive shift of all the levels, this is, however, a dynamically changing criterion, where the threshold depends on the intensity and hence on the depth and time in the simulation.

For clarity, the origin of the different terms in the equations will be stated briefly here followed by a more thorough elaboration on each of the terms in subsequent sections.

The first term is the strong-field ionization, $\dot{n}_{pi}(u)$, multiplied by a saturation factor, where n_{tot} is the total density of accessible electrons in the medium and $n_{\text{val}}=n_{\text{tot}}-\Sigma_j n_j$ is the electron density left in the valence band. W_{pl} is the plasma excitation rate, and α is the impact ionization rate.

The excitation rate α is multiplied with the saturation term and a sum over all the levels. The sum includes a Heaviside step function Θ where the argument depends on the excitation level in units of the photon energy and the corrected band gap, E_{corr}, of the material. This factor assures that impact ionization only occurs from levels where the electron energy is sufficiently high to fulfill both energy and momentum conservation. The Heaviside step function is multiplied with a "branch function" assuring that the energy for excitation of two electrons and a hole is distributed correctly to conserve the energy in the excitation process. The argument in the branch function contains a term defined as $\Delta E=\frac{1}{3}[j_{\text{crit}}-E_{\text{corr}}/(\hbar\omega_L)]$. A more detailed description is given in Sec. III B.

B. Ionization mechanisms

The primary mechanism for initiation of the excitation process in dielectric media is strong-field ionization, $\dot{n}_{pi}(u)$. For low intensities this can be described as a multiphoton process whereas at higher intensities tunnel ionization becomes the dominating process. An expression for the rate of strong-field ionization has been proposed by Keldysh[4] in both the mentioned regimes. As a wide range of electric field strengths is used in the calculations, a spline procedure has been applied to give a smooth transition between the multiphoton and the tunnel ionization regime as proposed originally by Kaiser *et al.*[6] This spline procedure is taking the region of validity of the two expressions into account. It should be noted that the values are strictly speaking unphysical outside the region of validity. However, the steps that appear on the multiphoton curve are physical as these show changes in the order of the multiphoton process owing to the ponderomotive shift, see Ref. 6.

Electron impact ionization can occur when the excited electrons gain sufficient energy to fulfill both energy and momentum conservation. The threshold energy for impact ionization is

$$E_{\text{imp}} = \frac{1+2\mu}{1+\mu} E_{\text{corr}}, \quad (9)$$

where μ is the electron mass in the conduction band relative to the hole mass in the valence band.[9] In these calculations μ has been set equal to one, meaning that the effective mass in the valence and conduction bands are assumed equal. This gives a threshold for impact ionization of $3/2E_{\text{corr}}$. In this expression E_{corr} is the corrected band-gap energy due to the ponderomotive energy (or the oscillation energy) in the strong electric field with $E_{\text{corr}}=E_{\text{gap}}+U_p$, where E_{gap} is the band gap of the dielectric material. From the calculations in Ref. 9, it can be seen that the statistically most probable process for impact ionization is when an electron with the threshold energy is colliding with a hole $1/6E_{\text{corr}}$ below the valence-band maximum, leading to two electrons with an energy of $1/6E_{\text{corr}}$ above the conduction-band minimum. In the simulations this has been implemented in the following way: when the energy is above the threshold for excitation, which is assured with the Heaviside step function Θ, an impact ionization event can occur with a rate given by α. If an electron is excited above the corrected band gap, the additional energy is distributed equally among the two electrons and the generated hole so that they each acquire ΔE as defined above. As the model consists of discrete levels, the two electrons are distributed in such a way that energy conservation will on average be fulfilled. This is ensured by the branch function in Eq. (8). In addition, saturation effects are again taken into account. The value of the impact ionization parameter in these calculations is set to $\alpha=10^{15}$ s^{-11}, but the results turn out to be relatively insensitive to the exact value of this parameter as long as it is much larger than the plasma-absorption rate. This is the case even for the highest intensities in the present simulations.

C. Optical properties of the material

To describe the plasma absorption and the propagation of the electromagnetic field into the material, knowledge about the optical properties of the material is required. The optical properties are governed by the complex refractive index, which can be determined from the density of excited electrons through the plasma frequency

$$\omega_p = \sqrt{\frac{e^2 \sum_j n_j}{m_e \epsilon_0}}, \quad (10)$$

where ϵ_0 is the permittivity in free space. The complex refractive index of the material is then given as

$$\tilde{k} = \sqrt{\left(k_0^2 + \frac{\omega_p^2}{\omega_l^2 - i\omega_l \Gamma}\right)}, \quad (11)$$

where k_0 is the refractive index of the dielectric material before excitation with the laser pulse.

The electron-scattering rate Γ is in general difficult to determine. It is here assumed to consist of contributions from electron-electron and electron-lattice collisions. In the present calculations the electron-lattice scattering rate is assumed energy independent with a value of $\Gamma_{e\text{-lat}}=5\times10^{15}$ s^{-1}, which is in reasonable agreement with calculations for SiO_2 for all but the lowest energies of the excited electrons.[10] For the electron-electron contribution, a classical gas collision rate is used, $\Gamma_{e\text{-}e}=4\pi\sqrt{2}r^2 v n$,[11] where r, v, and n are the radius, velocity, and density of the electrons, re-

spectively. In place of the classical radius for the electrons, the Debye screening length is used which can be written as $r^2=\frac{\epsilon_0 k_B T_e}{e^2 n}$.[6] This introduces the temperature T_e, which is approximated from the distribution between the excited levels even though the concept of temperature is questionable. It is assumed that an electron in a given energy level contributes $1/2k_BT$ for each degree of freedom according to the equipartition theorem. An approximate expression for the temperature can then be written as

$$\frac{3}{2}k_BT_e=\frac{\sum_j j\hbar\omega_l n_e(z,j)}{\sum_j n_e(z,j)}. \tag{12}$$

The average velocity v for the electrons is calculated classically as $v=\sqrt{\frac{3k_BT_e}{m_e}}$, where the kinetic energy is $3/2k_BT_e$. Note that only the random motion and not the collective motion caused by the ponderomotive energy is included in the expression for the temperature and the velocity, as the correlated motion in phase with the optical field does not contribute to the temperature. The final expression for the electron-electron-scattering rate is then

$$\Gamma_{e\text{-}e}=\frac{4\pi\epsilon_0}{e^2}\sqrt{\frac{6}{m_e}}(k_BT_e)^{3/2}. \tag{13}$$

Remarkably, the density of excited electrons does not enter explicitly in this equation, but the temperature is dependent on the excitation level of the electrons. The overall scattering rate is given as $\Gamma=\Gamma_{e\text{-lat}}+\Gamma_{e\text{-}e}$.

With a nonvanishing complex index of refraction κ, the intensity decays into the material. The losses in the optical field will lead to a spatially dependent heating of the electron plasma, which is determined by $\kappa(z)$.

To incorporate the plasma absorption the following parameter has been introduced to ease the notation:

$$W_{pl}=\frac{2\kappa\omega_l}{k}\frac{u}{\sum_{j<j_{\text{crit}}} n_j}. \tag{14}$$

This term is dependent on space and time through the refractive index in addition to the photon and electron densities. The expression is found by converting the plasma absorption per unit length, $2\kappa\omega_l u/c$, to absorption per unit volume and time by multiplication of the velocity, c/k. The sum over all the excited states in the denominator is included to facilitate expressions that are proportional to the density in level j. The plasma term is assumed to excite a number of electrons in each level which is proportional to the electron density in this level. This is done for all but the highest level in order to conserve the number of electrons.

D. Optical field

Immediately below the surface of the dielectric, no absorption losses have occurred, and the photon density is described by a Gaussian pulse in time,

$$u(t,z=0)=\frac{FT}{\hbar\omega_l c\tau}\sqrt{\frac{\ln 2}{\pi}}\exp\left[-(4\ln 2)\left(\frac{t-t_0}{\tau}\right)^2\right], \tag{15}$$

where F is the peak fluence, T the transmission into the sample, τ the full width at half maximum (FWHM) pulse duration of the Gaussian pulse, t_0 an offset relative to $t=0$ to allow integration over the pulse starting from $t=0$.

In the following, where the losses are introduced in the optical field, some approximations have been made in the description of the light to ease the computation. The approximations are based on the fact that the ablation depth is typically in the range of 1 μm or less, whereas a 100 fs laser pulse in vacuum has a spatial extent of 30 μm. Therefore, the intensity owing to the Gaussian envelope is assumed constant in space over the whole ablation region. However, as will be shown below, the losses depend strongly on the distance into the sample which will then give the spatial dependence of the incident light.

In addition, the losses are assumed constant on the timescale for the light to propagate into the material, which for 1 μm will correspond to approximately 3 fs. This approximation is exploited by assuming that the losses at the present time are identical to the conditions when the light passed through the outer region at earlier times. The correct method would be to consider the losses at previous times for regions in space closer to the surface, but the use of the present approximation eases the calculations tremendously.

The spatial derivative of the photon density can be written as

$$\frac{du}{dz}=-\left(\frac{2\kappa\omega_l}{c}+\frac{k}{c}\left[\frac{E_{\text{corr}}}{\hbar\omega_l}\right]\frac{\dot{n}_{pi}}{u}\frac{n_{\text{val}}}{n_{\text{tot}}}\right)u=-\beta u, \tag{16}$$

where the first term is the plasma absorption, which was discussed in Sec. III C, and the second term represents losses owing to multiphoton absorption. It is here assumed that each electron excitation is removing a number of photons equivalent to the order of the process.

The absorption can be divided into discrete spatial steps in the simulation by looking at the changes in the photon density by propagating a distance Δz,

$$u(z+\Delta z)=u(z)-\beta(z)u(z)\Delta z=[1-\beta(z)\Delta z]u(z). \tag{17}$$

The photon density in the depth z can then be expressed by the following equation:

$$u(t,z)=u(t,z=0)\prod_{i=1}^{[z/\Delta z]}[1-\beta(z_i)\Delta z], \tag{18}$$

where $u(t,z=0)$ is given by the loss-free photon density stated in Eq. (15), and $z_i=i\Delta z$ is the distance to the ith discrete spatial point. It should be noted that the transmission in Eq. (15) is not constant in time owing to the excitation of the material, but it can be calculated from the classical Fresnel expression using the time-dependent $\tilde{k}$ inside the material and $k=1$ outside the sample.

E. Technical details

In the simulations a Gaussian intensity distribution has been applied. The simulated depth is 2 μm, and no reflection of the light from the deepest point is included. The depth is subdivided into 100 spatial steps each 20 nm in thickness. The propagation time is 400 fs for pulse durations of 100 fs or shorter, with the laser pulse centered at 200 fs. For longer pulses the propagation time is four times the pulse duration with the maximum centered in the time interval. This will lead to an intensity which is 1.5×10^{-5} times the maximal intensity at the start of the simulation which will be negligible. As both plasma- and multiphoton absorptions are absent when the laser field goes to zero, only impact ionization from the highest levels can occur after the pulse is over. These levels are essentially depleted at a simulation time of four times the pulse duration if the electron excitation is not saturated, and the error by ending the simulation after this propagation time is negligible.

The fluences stated in the simulations are the peak fluences which in a comparison with experiments would correspond to

$$F = \frac{2E_{\text{pulse}}}{\pi\omega_0^2}, \tag{19}$$

where E_{pulse} is the pulse energy and ω_0 is the Gaussian beam waist.

Variations in three parameters have been performed in the simulation: the wavelength and pulse duration of the laser, and the band gap of the material. The basis in the simulations is a wavelength of 800 nm, a pulse duration of 100 fs, and a band gap of 5 eV. These parameters have then been varied subsequently.

The coupled differential equations for the electron densities are solved in MATLAB with the Ode45 solver which is adjusting the temporal subdivision in order to fulfill the required accuracy.

IV. RESULTS FROM THE SIMULATION

In this section, a presentation of the results from simulations of the multirate equations combined with a propagation of the optical field will be given. The consequences of variations in the wavelength, pulse duration, and the band gap of the material are presented. A discussion of the physics underlying the different changes with these parameters will be made.

A. Optical properties

In the theory for the optical field in Sec. III D an approximation was made where the spatial dependence was governed by losses and the temporal evolution was given by the envelope of the optical pulse. An example of the resulting photon density as a function of space and time can be seen in Fig. 1 for a 100 fs pulse centered at 800 nm in a 5 eV band-gap material with an applied fluence of 6.0 J/cm^2. For short times, the spatial dependence is almost constant as hardly any losses have been induced yet. When approaching the peak intensity, the spatial dependence becomes very pronounced owing to plasma- and multiphoton absorptions.

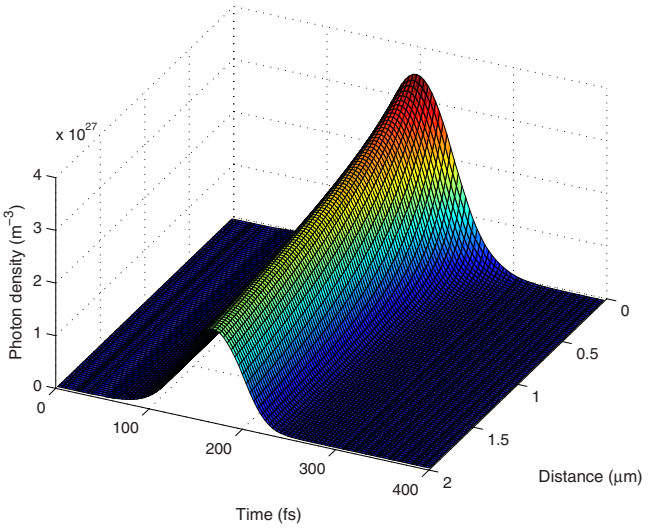

FIG. 1. (Color online) The photon density as a function of space and time for a 100 fs pulse centered at 800 nm in a medium with a 5 eV band gap. The incident fluence is 6.0 J/cm^2. Short times are representing the front end of the pulse where the spatial dependence is almost constant. At later times the absorption in the material leads to a spatial dependence of the photon density.

In the last part of the pulse, hardly any light is propagating significantly into the sample. This is *not* owing to a negligible transmission through the front surface, since the transmission after the end of the pulse in Fig. 1 is still 68%. Instead most of the light is absorbed by the excited material.

B. Ablation threshold criterion

Different approaches have been made to the ablation criterion in numerical simulations. Some models study the hydrodynamics after laser excitation and extract information about the formation of ejected fragments and the size distribution of these,[12] whereas another approach is to perform molecular-dynamics simulations.[13] A more simple practice is often followed, where a constant critical density is assumed as the ablation criterion.[14–17] However, the critical density is often determined from the criterion that the plasma frequency equals the laser frequency. For 800 nm light this can from Eq. (10) be determined to 1.74×10^{27} m^{-3}, which is close to a 2% criterion in the present work, 2×10^{27} m^{-3}. However, the condition of a critical plasma frequency implies a laser-frequency dependence of the critical density. The critical plasma density approach is based on the observation that the absorption increases significantly when this limit is reached and thereby ablation will occur. As the present model is already taking plasma absorption into account, it is considered unphysical to include this frequency dependence in the threshold criterion as well. Ablation is assumed to be caused by instabilities in the lattice owing to the high density of excited electrons and not due to properties of the optical field which is why a value independent of wavelength is chosen.

In Fig. 2 an example of the density of excited electrons as a function of depth can be seen in the upper panel. The three

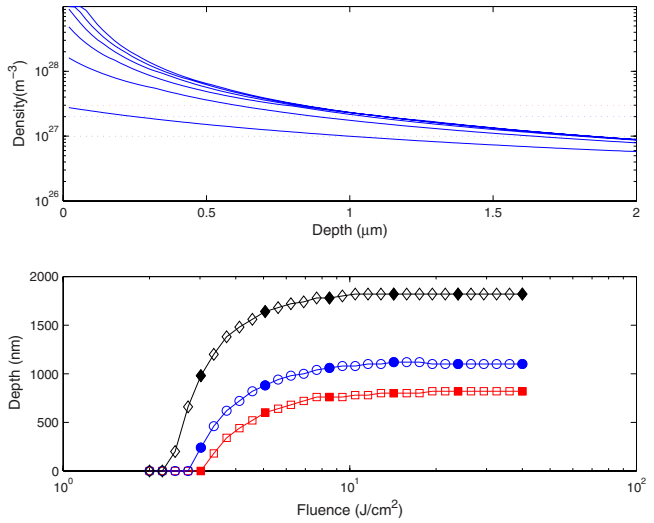

FIG. 2. (Color online) In the top panel the density of excited electrons as a function of the depth can be seen for different fluences. The dotted horizontal lines show ablation criteria of 1%, 2%, and 3% of the maximal electron density. The lower panel is showing the ablation depth as a function of fluence for the different ablation criteria. Black diamonds 1%, blue circles 2%, and red squares 3%. The filled symbols indicate the fluences depicted in the top panel.

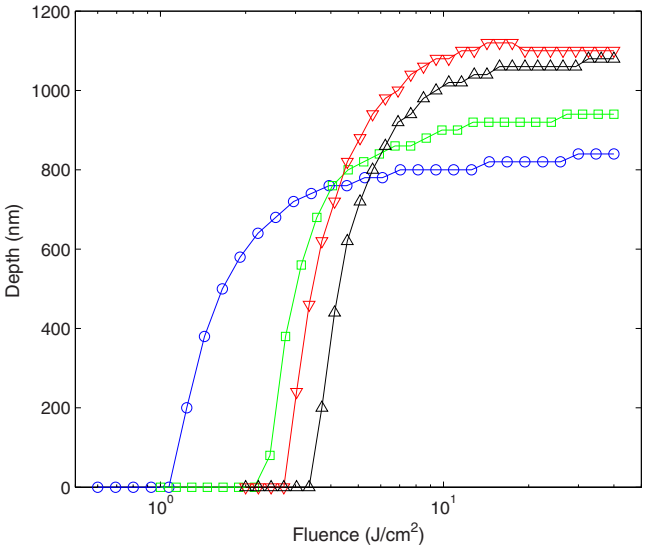

FIG. 3. (Color online) The ablation depth as a function of fluence for varying wavelengths. A pulse duration of 100 fs and a band gap of 5 eV has been maintained in all the simulations. The wavelength for the blue circles are 400 nm, green squares 530 nm, red down-pointing triangles 800 nm, and black up-pointing triangles are 1060 nm. The lines serve to guide the eyes.

horizontal dotted lines indicate thresholds of 1%, 2%, and 3%. In the lower panel the resulting ablation depths can be seen with the black diamonds corresponding to 1%, blue circles 2%, and the red squares 3%. A reduction to 1% can be seen to give a significantly larger ablation depth as compared to the higher threshold criteria. Note that the threshold fluence is varying much less than the depth in the simulations when the threshold criterion is varied. In a comparison with experiments, the threshold criterion will significantly influence the agreement, and this parameter should really be adjusted to best fit the data owing to the lack of a better model for the ablation criterion. In the rest of this paper, a threshold criterion of 2% is applied.

C. Wavelength dependence

The first parameter to vary is the wavelength of the incident laser. Simulations have been performed for wavelengths of 400, 530, 800, and 1060 nm and the results can be seen in Fig. 3. These wavelengths have been chosen as 800 nm is close to the maximal gain for Ti:sapphire and 400 nm is the frequency doubled of the fundamental. 1060 nm is near the central wavelength of Yb-doped fiber lasers and again 530 nm is the second harmonic of the output from these systems.

Two trends can be seen in Fig. 3 where a shorter wavelength leads to: (i) a lower ablation threshold, and (ii) a reduced ablation depth.

The first trend, where a lower threshold fluence is observed at lower wavelengths can be explained by a reduction in the order of the nonlinear process. This will facilitate multiphoton processes at lower fluences and generate seed electrons. An initiation of ablation at a lower fluence is therefore a consequence.

The second trend that long wavelengths lead to large ablation depths as compared to the short wavelengths can be explained by a comparison to metals. For metals the optical penetration depth is proportional to the wavelength. At high fluences where the ablation depth seems to saturate, the density of excited electrons becomes comparable to the density of conduction electrons in metals and the imaginary part of the refractive index is no longer negligible. This can explain the metal-like behavior at the high excitation levels. It should be noted that these two trends lead to a crossover in the ablation depth between the second harmonic and the fundamental.

D. Pulse-duration effects

Another relevant parameter in the ablation process is the laser-pulse duration. In Fig. 4 the pulse duration has been varied between 30 and 800 fs. A longer pulse duration can be seen to increase the ablation threshold as the maximum intensity is reduced for similar fluences and thereby less electrons are generated from multiphoton processes. However, the ablation depth seems to peak at a pulse duration near 100 fs. A further reduction in pulse duration gives high yields from the multiphoton process but only for a short period of time. Much heating of the electrons will be required for a further multiplication to occur owing to the large ponderomotive shift. When the pulses become longer than 100 fs, the balance between multiphoton excitation and multiplication of the excited electrons will change where the reduced peak intensity is leading to less seed electrons which cannot be compensated by the longer time for multiplication and the reduced ponderomotive shift.

In Fig. 5 the threshold fluence is shown as a function of the pulse duration on a log-log plot. The threshold depen-

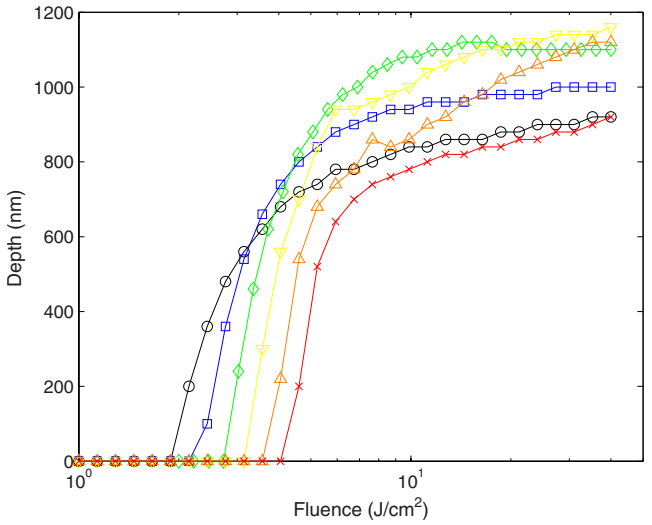

FIG. 4. (Color online) The ablation depth as a function of fluence for varying pulse durations. The following pulse durations can be seen in the figure: black circles 30 fs, blue squares 50 fs, green diamonds 100 fs, yellow down-pointing triangles 200 fs, orange up-pointing triangles 400 fs, and red crosses 800 fs. The wavelength in the simulations is 800 nm and a band gap of 5 eV has been applied.

dence on pulse duration appears to a good approximation to follow a piecewise power law. In the regime below 1 ps, the exponent is fitted to 0.24, whereas the simulated thresholds for pulse durations above 1 ps seem to fit well with an exponent of 0.15. For pulses longer than 10–100 ps, a $\tau^{1/2}$ dependence has previously been determined experimentally[5] owing to heat-diffusion effects. In the present investigation, the threshold is only simulated for pulse durations up to 25 ps as no diffusion effects are included in the model. In a systematic study by Mero *et al.*,[15] the threshold fluence has been found to scale as $F_{th} \propto \tau^{0.30}$, which is slightly higher

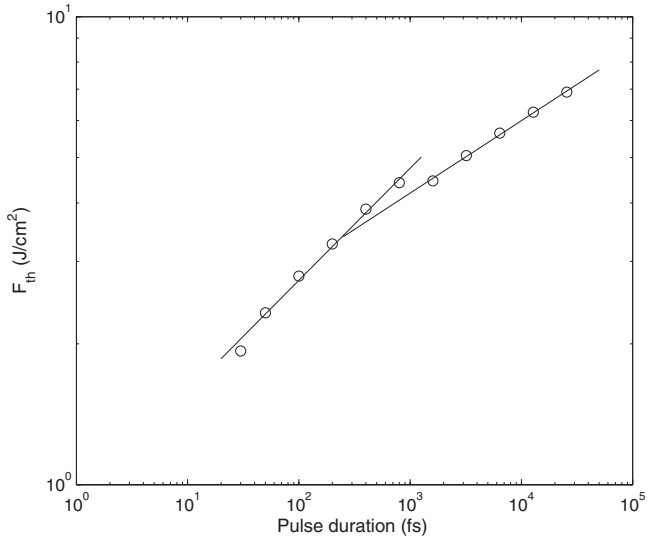

FIG. 5. The threshold fluence for varying pulse durations. The simulated threshold fluences have been fitted to a power-law function. The exponent is fitted to 0.15 in the regime above 1 ps and 0.24 below.

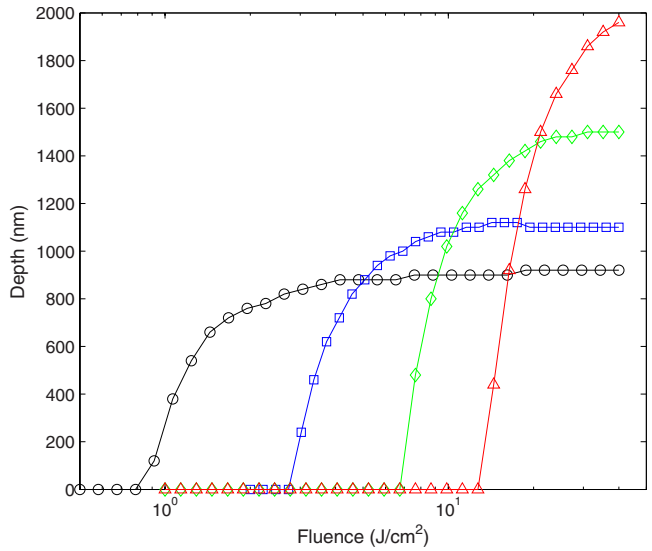

FIG. 6. (Color online) The ablation depth as a function of fluence for varying band gaps. The band gaps are: black circles 3 eV, blue squares 5 eV, green diamonds 7 eV, and red triangles 9 eV.

than seen in the simulations for the short pulse durations. However, Tien *et al.*[18] have in the short-pulse regime fitted their data to an exponent of 0.23 in excellent agreement with the present simulation. Experiments on SiO_2 performed by Giguère *et al.*[19] give an exponent as low as 0.12 for pulses shorter than 2 ps. This shows that the simulated results seem to lie well within the spread among the experiments.

The change in slope may imply regimes where different processes are dominating. At the shortest pulse durations the excitation mechanism is expected to be almost solely dependent on the strong-field ionization. As this process is strongly intensity dependent, shorter pulses are expected to give rise to a lower ablation threshold fluence. For slightly longer pulses other excitation mechanisms can no longer be neglected. This may be the second regime, where the slope is reduced compared to the strong-field ionization regime.

An important—and quite expected—lesson from the threshold dependence on the pulse duration is that for dielectric media the concept of fluence is no longer an adequate description of the optical pulse. In a thermal process as in metals, only the total energy of the pulse is of importance when the pulse duration is short compared to diffusion processes. For dielectrics the peak intensity is also relevant, as the process is initiated by a highly nonlinear multiphoton process.

The present method for describing laser ablation of dielectrics can readily be extended to describe the situation of pulses of a more complex pulse form. For instance recent investigations have demonstrated that complex pulse shapes can influence the ablation efficiency and reproducibility.[20,21]

E. Band-gap effects

The band gap is one of the parameters which have a major influence on both the ablation threshold and depth. Simulations for different band gaps can be seen in Fig. 6, where band gaps of 3, 5, 7, and 9 eV are shown. Low-band-gap

materials can be seen to have a low ablation threshold, which is in accordance with the results from the variation in the wavelength. Here a reduction in wavelength had a similar effect as both these effects can be ascribed to a lower order of the multiphoton excitation process. However, the two effects do not give identical results as the multiphoton ionization cross section and the ponderomotive shift are wavelength dependent.

In high-band-gap materials the calculated ablation depths become deeper than in low-band-gap materials. For a low-band-gap material, the multiphoton excitation starts rapidly at low fluences as the order of the process is relatively low. This leads to a fast increase in the electron density in the outermost layers, which will increase the absorption of the light and lead to plasma heating. The consequence is a short optical penetration depth due to the large imaginary part of the refractive index.

On the other hand, when the band gap is large, the optical field is permitted to propagate further into the material and at low fluences the density of excited electrons does not exceed the threshold anywhere in the material. When the fluence exceeds the threshold, a much larger depth will be excited due to the reduced slope in the excitation density and a larger ablation depth is the consequence. It should be noted that a crossover in the ablation depth appears when materials with different band gaps are processed.

This has experimentally been seen in dental ablation of calculus on root cement in Ref. 22. Calculus can here be considered a low-band-gap material, whereas the band gap is higher for the native root cement. A small therapeutic window is shown to be available below the ablation threshold for the root cement. However, the consequence of the crossover would be a fast ablation rate in the native root cement above the threshold of ablation, which is undesired. An application of the crossover phenomena would more realistically be possible in ablation of well ordered, layered materials where ablation only is desired in the uppermost low-band-gap material without damaging the lower-lying high-band-gap material.

If the ablation threshold is plotted as a function of the band gap, a power dependence seems to agree well with the data. This is shown in Fig. 7, where an exponent of 2.64 is obtained. This is slightly lower than would be expected if only multiphoton excitation is considered, as discussed in Ref. 23, where an exponent of 3 would then be expected. This confirms a dependence of other factors than solely multiphoton processes. The simulated results are in excellent agreement with data on BBS (barium aluminum borosilicate) made by Lenzner *et al.*,[24] where an exponent of 2.5 is obtained if a power-law dependence is assumed.

V. COMPARISON WITH EXPERIMENTS

Comparison of the simulated depths with experiments is a challenging task. Few depth measurements have been made on well-defined materials in single-shot experiments. In addition, as the pulse duration extends into the picosecond regime, the ablated structures can become split into two parts where shallow and more needlelike parts are seen.[25] Another

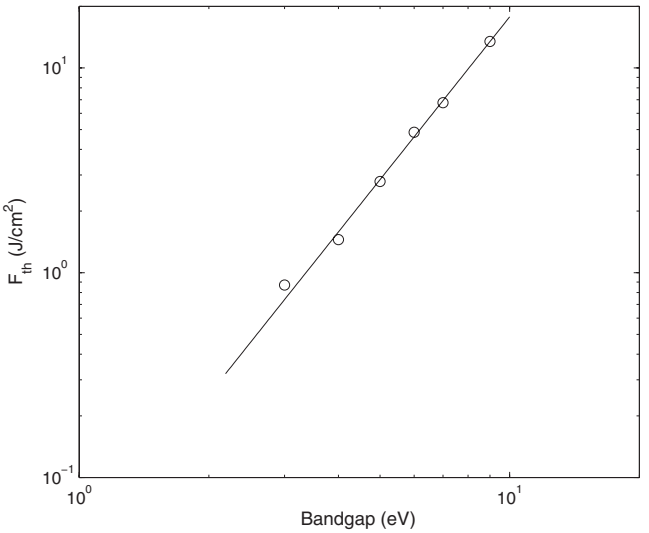

FIG. 7. Simulated thresholds for different band gaps. The applied pulse duration is 100 fs and a central wavelength of 800 nm has been applied. The threshold is to a good approximation scaling as a power law with the band gap with an exponent of 2.5.

approach applied in the literature is performing multishot ablation and extrapolating back to single-shot rates. However, this technique has an inherent weakness as it does not consider incubation effects, which are present already after the first shot.[26] Single-shot experiments have in the literature been performed on α-Al_2O_3,[25] where the band gap is stated to be 8.8 eV. The central wavelength of the laser is 800 nm and a pulse duration of 58 fs has been applied. These measurements can be seen in Fig. 8 as black dots, where the threshold has been found to 4.5 J/cm^2 and the depth is saturating near 350–400 nm at a fluence of 25 J/cm^2. This threshold has been confirmed at a pulse duration of 45 fs as well.[27]

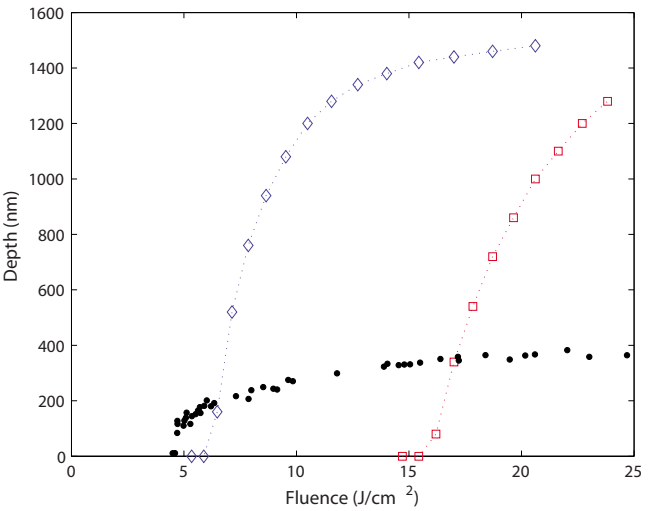

FIG. 8. (Color online) Experimental data from Ref. 25 are shown as black dots. The results of a simulation using the generic model with identical electron and hole masses and a 8.8 eV band gap can be seen as red squares. The blue diamonds are for a band gap of 6.48 eV and the electron and hole masses discussed in the text. Note, a linear fluence scale is applied.

Simulations at these conditions have been made for Al_2O_3 with a refractive index of 1.77. The result can be seen as red squares in Fig. 8, where the threshold and the ablation depth can be seen to be largely overestimated.

However, a theoretical calculation for α-Al_2O_3 has given a band gap of 6.48 eV, and effective electron and hole masses have been found to $0.38m_0$ and $3.99m_0$, respectively.[28] By insertion in Eq. (9), the barrier for fulfilling both energy and momentum conservation is then no longer $3/2E_{corr}$ but is reduced to $1.09E_{corr}$. Both these factors will reduce the threshold energy for impact ionization significantly and for large-band-gap materials, the effective masses should be considered, as this effect could change the order of the process significantly. A similar trend is seen for SiO_2, where electron and hole masses of $0.5m_0$ and $3m_0-10m_0$ are found.[29]

If simulations are made with the calculated parameters for Al_2O_3 better agreement between simulations and experiments can be found. The results are shown as blue diamonds in Fig. 8. The threshold is now reproduced significantly better, and the shape of the simulated and experimental data is similar. However, the ablated depth remains too deep compared with experiments.

In the literature, experiments can also be found for SiO_2 which has a comparable band gap. However, the ablation depth is here approaching 1 μm, and the threshold is reduced to a somewhat lower value of $2-3$ J/cm^2.[30] Both these trends are typical for lower-band-gap materials. This may mainly be owing to the extrapolation from five shots to the single-shot ablation applied by Ref. 30, which is inducing defects and thereby reduce the effective band gap, or alternatively due to a low purity of the applied material. Another contribution would be the low electron mass and large hole mass, which will enable energy conservation to be fulfilled for relatively low orders of the multiphoton process.

To achieve better agreement between the experimental and simulated ablation depths a systematic experimental study must be performed to make a more precise quantification of the ablation criterion. As was shown in Sec. IV B, the choice of the critical density is influencing the depth considerably.

VI. LIMITATIONS OF THE MODEL

The present model applies a steplike energy distribution for the electrons over the whole simulation time. This sounds like a severe limitation, since Ref. 6 demonstrates that such a distribution is smoothing already on a ~10 fs timescale. However, as pointed out also in Ref. 6, the effect is mainly a smearing and not a true redistribution of the electron energies. The applied model thus corresponds to employing a discretized continuum representation. The application of only a finite number of states is also not a serious approximation, as long as it is ensured that there is no accumulation of population in the uppermost level.

In the model no defects or structural changes leading to incubation have been included. These factors can affect the threshold fluence where, e.g., a threshold dependent on the beam radius is seen by Martin *et al.*[31] This is explained with a model including defects in the material, which will tend to lower the threshold fluence. In their model thresholds for both the defects and the native material are included. As no defects have been included in the present model, the threshold values in these simulations would correspond to the threshold for the native material, which may be higher than the experimentally measured values. As discussed in connection with the ablation-depth dependence on the band gap, the defects would tend to reduce the ablation threshold as these would act as inclusions of low-band-gap materials, which would tend to seed the absorption. Another relevant issue in a comparison between the simulation and experiments is that a spatially non-Gaussian pulse has been shown to reduce the measured threshold fluence as much as a factor of 2 on identical samples.[24,32] An extension of the model to include defects should include both defects, which are present at the start of the process, and light-induced effects such as, e.g., color centers.[26] Structural changes in the surface topography leading to a ripple pattern can also be observed in multishot experiments,[33] and the effect should be considered if the model should be extended to multishot ablation. Multishot experiments have previously been modeled where the propagation of the light has been included, and the density of free electrons is modeled with a single-rate equation.[16]

Another issue that has not been included in the present model is nonlinear propagation. If a spatially Gaussian pulse is applied, the intensity variations across the beam profile could induce effects such as self-focusing.[34] Neither this nor self-phase modulation are included in the present simulations, but these effects are expected to be negligible owing to the short propagation distance into the medium. In the model the spectral content of the pulse is assumed unchanged during the propagation, and in addition it is assumed meaningful only to consider the central wavelength of the pulse, which is questionable at the shortest obtainable pulses from Ti:sapphire lasers. If the model should be developed into a two- or three-dimensional model, the importance of these effects should be considered and eventually included. In addition, a description must include the hydrodynamics related to the highly excited dielectric and subsequent material transport.[35]

No diffusion effects in the electron system have been included in the present model. This is suggested to be done by assuming high excitation, which will give the insulator metal-like properties. An application of the two-temperature model[2,3] is then proposed as a method for including diffusion in the electron system.[36]

Other proposed models based on the single-rate equation for the excitation process of dielectrics include a decay term.[17,37] While the immediate effect of decay is of course to reduce the electron density, it cannot be concluded that this would lead to an increase in the ablation threshold. The energy of the decayed electrons is not lost, so in order to extend the model to include electronic decay, it will presumably be necessary to consider the energy-balance equations and apply a new ablation criterion.

The comparison with experiments in Sec. V indicates that the effective electron and hole masses are important and may have a significant influence in connection with the requirement of fulfilling both energy and momentum conservation

in the impact ionization process. To a lesser extent this will also influence the multiphoton ionization cross section. However, as discussed in some detail in Ref. 38, the effective-mass approximation may break down for wide-band-gap dielectrics at high excitation. In this case more general energy-momentum relations should be applied. Another consequence of the breakdown of the parabolic band description—that the effective band gap does not simply shift according to the ponderomotive potential—is also discussed in Ref. 38. These band-structure effects should be included in future extensions of the present model.

VII. SUMMARY

A numerical simulation of ablation processes in dielectric media has been performed. The model is founded on the multiple-rate equation and is extended with a propagation of the light into the material. The model is generic and is based on a few key parameters. Simulations have been made for varying laser wavelengths and pulse durations as well as for different band gaps of the materials. The observed dependencies and their underlying physical explanation have been discussed.

*Also at Danish Technological Institute, Kongsvang Allé 29, 8000 Aarhus C, Denmark.
†balling@phys.au.dk

[1] B. Rethfeld, Phys. Rev. Lett. **92**, 187401 (2004).
[2] S. I. Anisimov, B. L. Kapeliovich, and T. L. Perel'man, Sov. Phys. JETP **39**, 375 (1974).
[3] B. H. Christensen, K. Vestentoft, and P. Balling, Appl. Surf. Sci. **253**, 6347 (2007).
[4] L. V. Keldysh, Sov. Phys. JETP **20**, 1307 (1965).
[5] B. C. Stuart, M. D. Feit, A. M. Rubenchik, B. W. Shore, and M. D. Perry, Phys. Rev. Lett. **74**, 2248 (1995).
[6] A. Kaiser, B. Rethfeld, M. Vicanek, and G. Simon, Phys. Rev. B **61**, 11437 (2000).
[7] T. Otobe, M. Yamagiwa, J.-I. Iwata, K. Yabana, T. Nakatsukasa, and G. F. Bertsch, Phys. Rev. B **77**, 165104 (2008).
[8] B. Rethfeld, Phys. Rev. B **73**, 035101 (2006).
[9] B. K. Ridley, *Quantum Processes in Semiconductors* (Clarendon, Oxford, 1982).
[10] D. Arnold, E. Cartier, and D. J. DiMaria, Phys. Rev. B **45**, 1477 (1992).
[11] F. Reif, *Fundamentals of Statistical and Thermal Physics* (McGraw Hill, Singapore, 1965).
[12] T. E. Glover, J. Opt. Soc. Am. B **20**, 125 (2003).
[13] R. F. W. Herrmann, J. Gerlach, and E. E. B. Campbell, Appl. Phys. A: Mater. Sci. Process. **66**, 35 (1998).
[14] B. C. Stuart, M. D. Feit, S. Herman, A. M. Rubenchik, B. W. Shore, and M. D. Perry, Phys. Rev. B **53**, 1749 (1996).
[15] M. Mero, J. Liu, W. Rudolph, D. Ristau, and K. Starke, Phys. Rev. B **71**, 115109 (2005).
[16] J. R. Vázquez de Aldana, C. Méndez, L. Roso, and P. Moreno, J. Phys. D **38**, 2764 (2005).
[17] E. Louzon, Z. Henis, S. Pecker, Y. Ehrlich, D. Fisher, M. Fraenkel, and A. Zigler, Appl. Phys. Lett. **87**, 241903 (2005).
[18] A.-C. Tien, S. Backus, H. Kapteyn, M. Murnane, and G. Mourou, Phys. Rev. Lett. **82**, 3883 (1999).
[19] D. Giguère, G. Olivié, F. Vidal, S. Toetsch, G. Girard, T. Ozaki, J.-C. Kieffer, O. Nada, and I. Brunette, J. Opt. Soc. Am. A Opt. Image Sci. Vis **24**, 1562 (2007).
[20] J. R. Gulley, S. W. Winkler, and W. M. Dennis, Opt. Eng. **47**, 054302 (2008).
[21] L. Englert, M. Wollenhaupt, L. Haag, C. Sarpe-Tudoran, B. Rethfeld, and T. Baumert, Appl. Phys. A: Mater. Sci. Process. **92**, 749 (2008).
[22] J. F. Kraft, K. Vestentoft, B. H. Christensen, H. Løvschall, and P. Balling, Appl. Surf. Sci. **254**, 1895 (2008).
[23] P. G. Eliseev, O. N. Krokhin, and I. N. Zavestovskaya, Appl. Surf. Sci. **248**, 313 (2005).
[24] M. Lenzner, J. Krüger, S. Sartania, Z. Cheng, C. Spielmann, G. Mourou, W. Kautek, and F. Krausz, Phys. Rev. Lett. **80**, 4076 (1998).
[25] S. Guizard, A. Semerok, J. Gaudin, M. Hashida, P. Martin, and F. Quéré, Appl. Surf. Sci. **186**, 364 (2002).
[26] A. Hertwig, S. Martin, J. Krüger, and W. Kautek, Appl. Phys. A: Mater. Sci. Process. **79**, 1075 (2004).
[27] X. Li, T. Jia, D. Feng, and Z. Xu, Appl. Surf. Sci. **225**, 339 (2004).
[28] J. E. Medvedeva, E. N. Teasley, and M. D. Hoffman, Phys. Rev. B **76**, 155107 (2007).
[29] M. I. Vexler, S. E. Tyaginov, and A. F. Shulekin, J. Phys.: Condens. Matter **17**, 8057 (2005).
[30] T. Q. Jia, Z. Z. Xu, X. X. Li, R. X. Li, B. Shuai, and F. L. Zhao, Appl. Phys. Lett. **82**, 4382 (2003).
[31] S. Martin, A. Hertwig, M. Lenzner, J. Krüger, and W. Kautek, Appl. Phys. A: Mater. Sci. Process. **77**, 883 (2003).
[32] W. Kautek, J. Krüger, M. Lenzner, S. Sartania, C. Spielmann, and F. Krausz, Appl. Phys. Lett. **69**, 3146 (1996).
[33] F. Costache, M. Henyk, and J. Reif, Appl. Surf. Sci. **186**, 352 (2002).
[34] S. S. Mao, F. Quéré, S. Guizard, X. Mao, R. E. Russo, G. Petite, and P. Martin, Appl. Phys. A: Mater. Sci. Process. **79**, 1695 (2004).
[35] E. G. Gamaly, S. Juodkazis, K. Nishimura, H. Misawa, B. Luther-Davies, L. Hallo, P. Nicolai, and V. T. Tikhonchuk, Phys. Rev. B **73**, 214101 (2006).
[36] I. M. Burakov, N. M. Bulgakova, R. Stoian, A. Rosenfeld, and I. V. Hertel, Appl. Phys. A: Mater. Sci. Process. **81**, 1639 (2005).
[37] M. Li, S. Menon, J. P. Nibarger, and G. N. Gibson, Phys. Rev. Lett. **82**, 2394 (1999).
[38] V. E. Gruzdev, Phys. Rev. B **75**, 205106 (2007).